PHYSICAL REVIEW E **70**, 011405 (2004)

Kinetics of phase transformations in depletion-driven colloids

Juan J. Cerdà,[1,2] Tomás Sintes,[1] C. M. Sorensen,[2] and A. Chakrabarti[2]
[1]*Departament de Física and IMEDEA (CSIC-UIB), Universitat de les Illes Balears and Consejo Superior de Investigaciones Científicas, 07122 Palma de Mallorca, Spain*
[2]*Department of Physics, Cardwell Hall, Kansas State University, Manhattan, Kansas 66506-2601, USA*
(Received 19 February 2004; published 26 July 2004)

We present results from a detailed numerical study of the kinetics of phase transformations in a model two-dimensional depletion-driven colloidal system. Transition from a single, dispersed phase to a two-phase coexistence of monomers and clusters is obtained as the depth of the interaction potential among the colloidal particles is changed. Increasing the well depth further, fractal clusters are observed in the simulation. These fractal clusters have a hybrid structure in the sense that they show hexagonal closed-packed crystalline ordering at short length scales and a ramified fractal nature at larger length scales. For sufficiently deep potential wells, the diffusion-limited cluster-cluster aggregation model is recovered in terms of the large-scale fractal dimension D_f of the clusters, the kinetic exponent z, and the scaling form of the cluster size distribution. For shallower well depths inside the two-phase coexistence region, simulation results for the kinetics of cluster growth are compared with intermediate-stage phase separation in binary mixtures. In the single-phase region, growth kinetics agree well with a mean-field aggregation-fragmentation model of Sorensen, Zhang, and Taylor.

DOI: 10.1103/PhysRevE.70.011405 PACS number(s): 82.70.Gg, 82.70.Rr

I. INTRODUCTION

The general problem of how a dispersed phase, such as particles in a colloid or molecules in a solution, come together, when destabilized, to form a condensed phase, such as aggregates, gels, or precipitated crystalline solids, is of fundamental importance for controlling the assembly of the dispersed phase into a useful material [1]. Parts of this grand problem have seen considerable previous research, such as irreversible aggregation [2] and the formation of fractal aggregates [3], gelation, spinodal decomposition [4], nucleation, and early studies of growth during precipitation [5]. However, a general theory that encompasses all of these related phenomena is lacking.

Colloidal solutions can display a rich series of phase transitions between gas, liquid, and solid phases [6,7]. The liquid phase can be amorphous or liquid crystalline, and the solid phases can be crystalline, amorphous (perhaps fractal), and gel. These possibilities are controlled by the potential between the disperse components and the kinetics of the phase transition. A fluid-to-crystal transition occurs if the potential is solely hard sphere. The addition of an attractive potential brings on three-phase equilibria. A key parameter that causes large changes in the phase diagram is the relative range of the attractive interaction between the colloidal particles. As the relative range of the attractive interaction lessens, the system develops a gas-crystalline coexistence with a metastable liquid-liquid coexistence region.

A theoretical understanding of the colloidal phase diagram leads to better control of colloidal growth kinetics. For example, colloidal aggregation, which is often irreversible, can be made reversible on experimental time scales by tailoring both the strength and range of interaction between colloidal particles. Reversible aggregation of colloids is known to exhibit various intriguing phenomena [6,7], such as transient gel formation, compactification, and crystallization. Moreover, reversible aggregation has a striking similarity with other phase changes, such as spinodal decomposition and the formation of precipitated crystalline solids from solutions. A quantitative understanding of reversible aggregation is thus needed for a unifying description of the transition from a general dispersed phase to clusters, and for a greater control over the self-assembly and material properties of various colloids.

Manipulation of the interaction potential between colloidal particles can be achieved in several ways. For a charge-stabilized colloidal solution, this can be done by the addition of salt or surfactant solution so that a *secondary minimum* [8] in the interaction potential forms. Another way to control the interaction potential between colloidal particles is to induce a depletion interaction by adding a nonadsorbing polymer [9–11] (or a different sized colloid [12]) in an otherwise stable colloidal solution. A major advantage of the latter systems is that the strength and range of the depletion interaction can be easily controlled by varying the polymer concentration and the length of the added polymer chains.

The phase behavior of depletion-driven colloids has been studied extensively both theoretically and experimentally. The equilibrium behavior of these systems being reasonably well understood, much of the recent work has been directed to understanding the kinetics of phase transitions [12,13] and colloidal gelation [14] (and its relation to glass transition[15] and the more general jamming transition [16]) in these systems. Hobbie [12] has studied growth kinetics of the crystallization process in depletion-driven colloids and compared the experimental results with mean-field theories of aggregation fragmentation. Direct observation of crystallization and aggregation has been carried out more recently by de Hoog *et al.* [13] by varying the polymer concentration, hence the depth of the depletion potential. Brownian dynamics simulations [17–20] have also been carried out to study transient gel formation and crystallization in these systems. In particular, Soga, Melrose, and Ball [17,18] (SMB) have observed a variety of nonequilibrium behaviors in their simulations by

varying the strength of the depletion potential. Evidences of metastability, homogeneous nucleation, kinetically arrested gel state, and density instability were reported by SMB in their simulations. The use of computer simulations to study aggregation kinetics in these systems is particularly useful, as one can avoid sedimentation-related complications seen in experiments.

In this paper, we present the results from extensive Brownian dynamics simulations for a system of colloidal particles interacting via the depletion potential. We assume that the depletion interaction can be approximately accounted for by an effective two-body interaction between a pair of colloidal particles, as suggested by Asakura-Oosawa [9] and Vrij [10]. In contrast to SMB, we focus on lower monomer concentration (far away from the percolation threshold) and restrict ourselves to two dimensions. This allows us to carry out a detailed comparison of the cluster morphology and aggregation kinetics to traditional models of aggregation and fragmentation. Clusters obtained in the simulations range from dense, faceted crystals to fractal aggregates, which show ramified morphology on large scales but hexagonally packed crystalline morphology on short length scales. Increasing the depth of the depletion potential well, a transition from a dispersed phase to a coexistence of dispersed and solid phase is found. Near the transition point, a formation of clusters with a round shape is observed. As the well depth is increased further, one first obtains elongated clusters, and then fractal clusters form for deep enough well depths. Our simulations also show how growth kinetics evolve from the irreversible limits to systems which come to equilibrium over the simulation time due to fragmentation.

The rest of the paper is organized as follows. In Sec. II we describe the model and numerical method employed in our work. In Sec. III we present simulation results and compare them with traditional aggregation, aggregation-fragmentation, and phase separation models. Finally, we conclude in Sec. IV with a brief summary and discussion of the results.

II. NUMERICAL MODEL

In our Brownian dynamics simulations [21], we consider a two-dimensional (2D) system of linear size $L=256\sigma$ containing $N_m=13,107$ colloidal particles of mass m and diameter σ. This sets the monomer area fraction to be $f_v \approx 0.157$. We also set $m=1$ and $\sigma=1$, and measure all distances in units of σ. Periodic boundary conditions are enforced to minimize wall effects. The equations of motion for the colloidal particles read as

$$\ddot{\vec{r}}_i = -\vec{\nabla} U_i - \Gamma \dot{\vec{r}}_i + \vec{W}_i(t), \tag{1}$$

where Γ is the monomer friction coefficient and $\vec{W}_i(t)$, which describes the random force acting on each colloidal particle, is a Gaussian white noise with zero mean and satisfies the 2D fluctuation-dissipation relation $\langle \vec{W}_i(t) \cdot \vec{W}_j(t') \rangle = 4k_B T \Gamma \delta_{ij} \delta(t-t')$. Hydrodynamic interactions, including lubrication forces, are ignored in the simulation as they might not be of predominant importance for a study of quiescent secondary minimum colloids [22]. The potential U acting upon each colloidal particle has a twofold contribution: the two-body depletion potential of Asakura-Oosawa (U_{AO}), plus a repulsive hard-core-like interaction (U_{hc}) given by the following expressions,

$$\frac{U_{AO}(r_{ij})}{k_B T} = \left\{ \begin{array}{ll} \dfrac{3\phi_P}{2\zeta^3}\left[(1+\zeta)^2 r_{ij} - \dfrac{1}{3} r_{ij}^3 - \dfrac{2(1+\zeta)^3}{3} \right], & \text{for } r_{ij} < (1+\zeta) \\ 0, & \text{for } r_{ij} > (1+\zeta) \end{array} \right\}, \tag{2}$$

and

$$\frac{U_{hc}(r_{ij})}{k_B T} = r_{ij}^{-n}. \tag{3}$$

In Eq. (2), ζ is the size ratio between a polymer chain and a colloidal particle, and is set equal to $\zeta=0.1$ as in previous works [17,18]. Thus the interaction is quite short ranged and is cut off at a reduced distance of 1.1. ϕ_P is the polymer volume fraction which controls the strength of the depletion interaction in the Asakura-Oosawa model. In the hard-core-like repulsive interaction given by Eq. (3), we have set $n=36$. Exponents $n<36$ are reported [23] to lead to anomalies when a hard-core mimic is required in the potential. The total pair potential $U=U_{AO}+U_{hc}$ passes through a minimum value (U_m) which is related to the polymer volume fraction ϕ_P, as tabulated in Table I. In what follows, we will characterize the strength of the potential in terms of the absolute value of the minimum potential depth, $|U_m|$, instead of the polymer volume fraction ϕ_p. We choose $\Gamma=0.5$, and a time step $\Delta t=0.005$ in reduced time units of $\sigma(m/U_m)^{1/2}$ with mass $m=1$. All simulations start from a random initial monomer conformation and the results for the kinetics are averaged over more than 100 runs.

III. RESULTS

A. Cluster morphology

Transition from a single, dispersed phase to a state in which the solid phase starts to develop in the two-phase region is observed in the simulations when $|U_m|$ is larger than

TABLE I. Relation between nonadsorbing polymer volume fraction ϕ_p and the absolute value ($|U_m|$) of the total interacting potential U.

ϕ_p	$\lvert U_m\rvert / k_BT$
0.1768	2.000
0.2110	3.000
0.2262	3.125
0.2266	3.135
0.2314	3.250
0.2410	3.500
0.2610	4.000
0.2800	4.500
0.2980	5.000
0.3330	6.000
0.3670	7.000

a critical value U_c. From our simulations, we estimate that $U_c \approx 3.130 k_BT$ for our choice of monomer area fraction f_v. For smaller values of $|U_m|$, small *fluctuating clusters* in the dispersed phase form and dissolve over some correlation time. The linear size of these fluctuations increases as one approaches the transition. This is expected as the correlation length in the single phase should increase as a power law near a critical point. A phase diagram for the model considered here is known accurately in three dimensions [24], but not in two dimensions. For this reason, a quantitative identification of the quench points chosen in our work on the 2D phase diagram is not possible.

For computing cluster properties, we consider two neighboring particles to belong to the same cluster if the distance between their centers is less than or equal to the range of the interaction, i.e., $1+\zeta$ (or 1.1 for our choice of ζ) in units of σ. Figure 1 shows a snapshot for a system with $|U_m| = 3.125 k_BT$. In this case the system is in the single phase as $|U_m| < U_c$ and the largest observed fluctuating cluster has a size of less than 100 particles. As shown in the inset of Fig. 1, these small clusters have amorphous structures. No evidence of crystal formation is found in these clusters. If we set $|U_m|$ close to the critical value, but slightly deeper than U_c, the nucleation and growth of round clusters occur. The growth of only one round-shaped cluster in our finite-sized simulation box is observed in Fig. 2 for $|U_m| = 3.135 k_BT$. This value of $|U_m|$ puts the system barely in the two-phase region.

Increasing the depth of the potential well $|U_m|$ further, nucleation becomes more heterogeneous in our simulation box, as can be seen in the top-left snapshot of Fig. 3 for $|U_m| = 3.25$ at an early time. For this value of $|U_m|$, large round-shaped clusters in a sea of monomers (and small clusters) are observed at late times (left column of Fig. 3). The average coordination number per particle inside such a cluster is close to 6, and as shown in Fig. 4(c), hexagonal packing of the particles is clearly present inside the cluster. In Fig. 4, details of cluster shapes are shown for several values of the potential well depth. Once two clusters collide with each other, the shape of the newly formed cluster remains anisotropic for some time while it evolves toward a circular

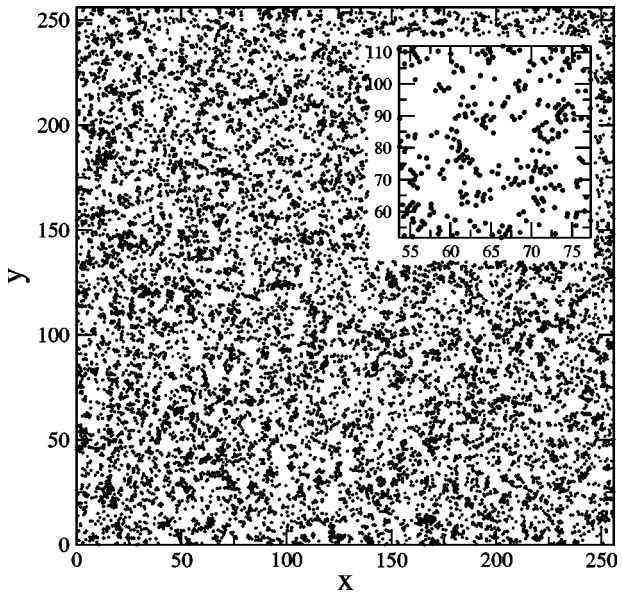

FIG. 1. Snapshot of the simulated colloidal system at $t = 10\,000$. Here, the well depth is set to $|U_m| = 3.125$. the system is in the single-phase region and the dispersed phase is observed.

shape to reduce interfacial energy. During this course, the resulting cluster bears the history of the collision in its shape [such as in the ordering of single crystal domains inside the cluster as in Fig. 4(e)]. The timescale for this shape evolution depends critically on the potential well depth $|U_m|$, as we will see shortly.

Increasing the degree of quenching into the two-phase region by setting $|U_m| = 4.0 k_BT$, rather elongated clusters that grow with time are seen (Fig. 3, central column). In this case, the potential well is deep enough to slow down the movement of monomers on a cluster surface, which is needed for

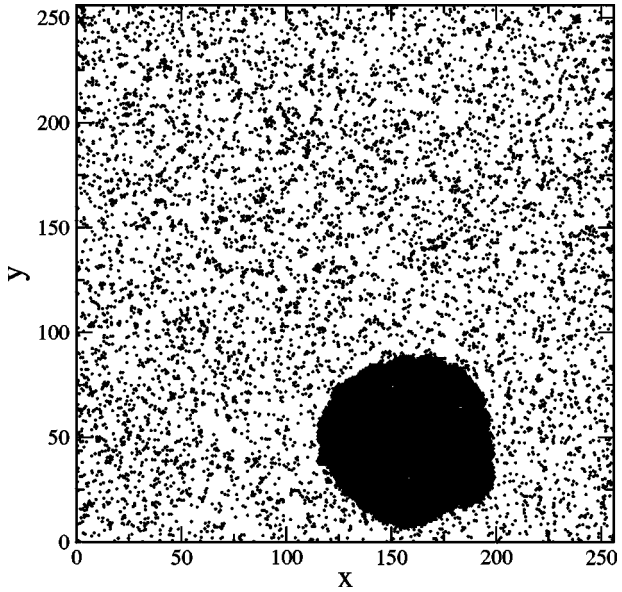

FIG. 2. Snapshot of the simulated colloidal system at $t = 10\,000$ for $|U_m| = 3.135$. A single round-shaped cluster is growing in the simulated box surrounded by the dispersed phase.

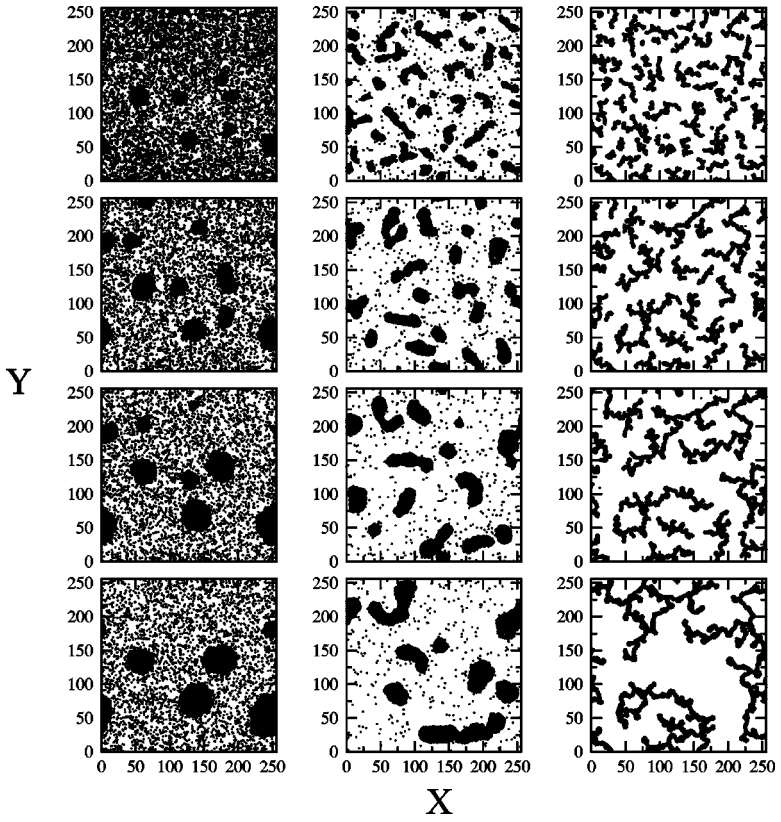

FIG. 3. Temporal evolution for three different quenches. The first column shows snapshots at $t=3000$, 6000, 23 000 and 40 000 for $|U_m|=3.25$. The second column shows snapshots at $t=3000$, 20 000, 43 000, and 84 000 for $|U_m|=4.0$. The third column shows snapshots at $t=1000$, 3000, 10 000, and 86 000 for $|U_m|=7.0$. Cluster morphology shows a distinct change as the depth of the potential is varied.

a reduction of interfacial energy. Therefore, new collisions are produced before anisotropic clusters formed from previous collisions have enough time to reshape themselves into circular clusters. As a result, the clusters seen in this case are elongated even at very late times. For an even larger well depth, such as $|U_m|=7.0k_BT$ (Fig. 3, right column), fractal clusters are obtained. We speculate that the interfacial tension-driven surface reorganization of monomers is almost frozen in this case, and the cluster shape results mainly from random cluster-cluster collisions as in a traditional diffusion-limited cluster-cluster aggregation (DLCA) or reaction-limited cluster-cluster aggregation (RLCA) models. However, even for this deep well depth, the aggregates show hexagonal closed-packed crystalline ordering at short length scales [Fig. 4(f)], while displaying ramified fractal nature at larger length scales. To be specific, this cluster morphology cannot be reproduced by a traditional DLCA modeling for which the typical coordination number of a particle in a cluster is ≈ 2. Large-scale morphology of the simulated clusters display close similarities with aggregates observed experi-

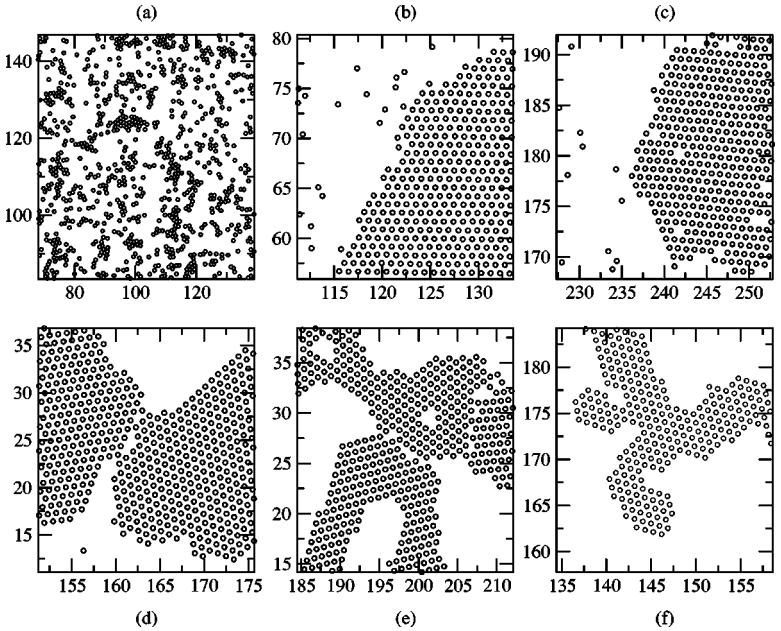

FIG. 4. Details of cluster morphology for several values of the potential well depth. From top left to bottom right, we show the results for $|U_m|=3.125$(a), 3.135(b), 3.25(c), 4.0(d), 5.0(e), and $7.0k_BT$(f), respectively. Cluster morphology for $|U_m|=3.125$ shows a dispersed phase with noncrystalline structures (a). For well depths larger than the transition value $U_c \simeq 3.130$, particles are arranged hexagonally inside the clusters. When collision between two clusters is recent, the history of such a collision can be seen in the resultant cluster shape.

mentally by de Hoog *et al.* [13] and Anderson *et al.* [25] in the earlier stages of the aggregation in depletion-driven colloids, before sedimentation becomes crucial. It should be noted here that such a mixed morphology of aggregating clusters was observed by Skjeltorp [26] in 2D aggregates of polystyrene spheres attracting via a secondary minimum. In such a system, the superposition of a screened electrostatic repulsion and a van der Waals attraction leads to the formation of a secondary minimum [8,27] in the potential, with a rather high energetic barrier between the primary and secondary minima. The barrier between these minima prevents irreversible aggregation and these charged colloids can effectively interact through the secondary minima.

B. Comparison with traditional models of aggregation and phase separation

1. Fractal dimension

The next step in our analysis is to carry out a quantitative comparison of the results from Brownian dynamics simulations with more traditional models, such as DLCA and RLCA. These limiting nonequilibrium models have been quite successful in describing aggregation. In DLCA, the rate-limiting step is the Brownian diffusion by which the particles meet and stick irreversibly, and in RLCA, the limiting step is the small probability of clusters sticking when they touch. A general feature of such irreversible processes is that the resulting structures are fractals with characteristic fractal dimensions. However, if the magnitude of the interaction potential between colloidal particles is comparable to thermal energy k_BT, both rearrangement and fragmentation (hence reversible aggregation) of clusters can take place. In such situations, one needs to compare the results of current Brownian dynamics simulations with models that consider both aggregation and fragmentation.

The large length scale cluster morphology obtained in our simulations is quantified by computing the cluster-ensemble averaged fractal dimension D_f. This is achieved by writing $N \sim R_g^{D_f}$, where R_g is the radius of gyration of an individual cluster containing N particles. Figure 5 shows the temporal evolution for the fractal dimension in two representative cases. Computation of the fractal dimension confirms a transition from compact clusters with $D_f=2$ to fractal clusters when we increase the well depth. We find that the fractal dimension for a large potential well depth is given by $D_f \simeq 1.4$. Within the statistical error of our data, this value of D_f is the same as the fractal dimension obtained in 2D DLCA models. Thus, Brownian dynamics simulations for a deep well depth reproduce the DLCA limit in terms of the large-scale fractal dimension, even though the short length scale structure of the clusters are totally different in these two models.

2. Growth kinetics

Since the potential well depth dictates cluster morphology, it is expected to control cluster growth kinetics as well. We have studied three different regimes (or "quench depth" using terminology of fluid-fluid phase separation) of growth kinetics: deep potential well depth (deep quench in the two-phase region), shallow potential well depth (shallow quench in the two-phase region), and quenches in the single-phase region.

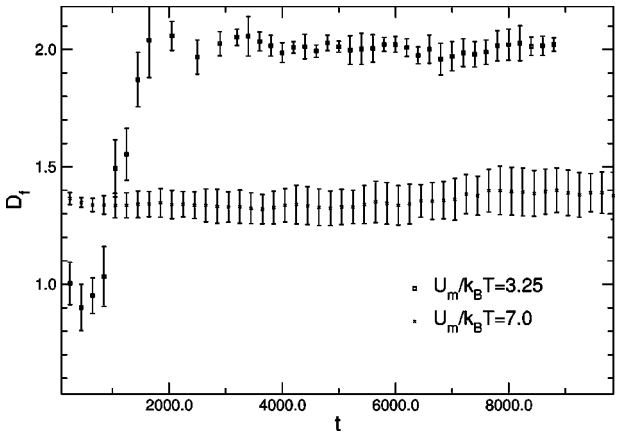

FIG. 5. Time evolution of the cluster averaged fractal dimension, D_f for well depths $|U_m|=3.25$ and $7k_BT$. For the lower value of $|U_m|$, compact clusters are found for which the fractal dimension is close to 2. We have calculated the fractal dimension as a function of time, including only clusters with a size equal or higher than 10% of the size of the largest cluster in the system. Inclusion of too small clusters produces a slight bias of the slope, which results in D_f being larger than 2. When increasing $|U_m|$, a gradual transition to fractal clusters is observed. Fractal clusters for $|U_m|=7k_BT$ have a fractal dimension of $D_f \simeq 1.4$, close to the 2D DLCA result.

(a) Deep quench in the two-phase region. We compute the mean size of clusters $s(t)$ (as the number of monomers per cluster) and the cluster-size distribution $n(N)$. The kinetic theory based on the Smoluchowski equation predicts that for irreversible aggregation at late times,

$$s(t) \sim t^z, \tag{4}$$

where z is the kinetic exponent that depends on the homogeneity constant, λ, of the aggregation kernel,

$$z = 1/(1-\lambda). \tag{5}$$

For the DLCA model with a Brownian coagulation kernel, a scaling argument [28,29] yields $\lambda=(d-3)/D_f$ in the dilute limit. In three dimensions, this provides $\lambda=0$ and $z=1$ as expected [2]. In two dimensions, however, this leads to $\lambda=-1/D_f=-0.7$ with $D_f=1.4$ and hence $z=0.59$ in the dilute limit.

Another factor that influences growth kinetics of fractal aggregates is the *volume fraction occupied by the clusters*, f_v^c. Since the fractal dimension D_f of the clusters is less than the space dimension d, f_v^c increases throughout aggregation, and evolution to a crowded state takes place. f_v^c can be computed in terms of the perimeter radius of the clusters which, is related to the cluster radius of gyration R_g. Thus, cluster crowding can be understood by considering the ratio of the cluster center of mass to the cluster nearest-neighbor center-of-mass separation R_{nn}, to the cluster radius-of-gyration R_g, which scales with time as $R_{nn}/R_g \propto t^{-z(d-D_f)/(dD_f)}$. Note that $R_{nn}/R_g \to 0$ at late times, indicating gelation occurring in the

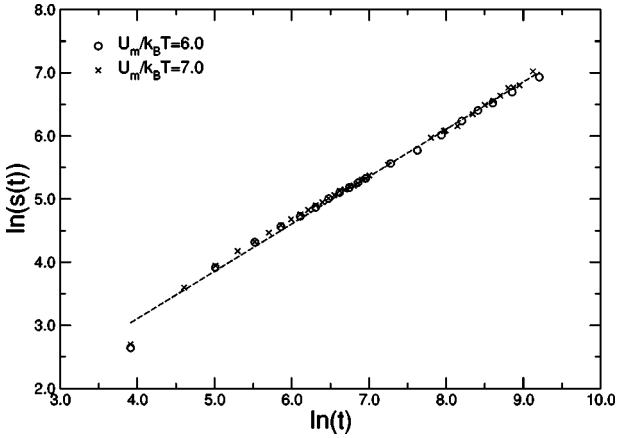

FIG. 6. Log-log plot for time evolution of the averaged cluster size for deep well depths. The kinetic exponent, z, obtained from linear fits, is given by 0.74 ± 0.05 in each case.

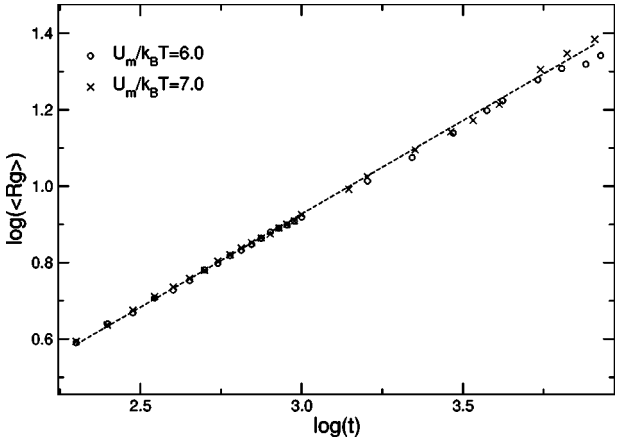

FIG. 7. Log-log plot of radius of gyration vs time for deep well depths. The exponent, $a = z/D_f$, obtained from linear fits, is given by 0.52 ± 0.04 in each case.

system. In practice, however, the system gels well before this condition is reached as the clusters are ramified. It is known that the kinetic exponent z increases as the system gets dense [30], i.e, as the cluster volume fraction f_v^c increases. For an intermediate value of f_v^c, scaling arguments [28] yield $z \simeq 1.28$ in three dimensions and $z \simeq 0.67$ in two dimensions.

Our results for $s(t)$ vs t for deep potential wells (such as with $|U_m| = 6.0$ and $7.0 k_B T$) are presented in Fig. 6 as a log-log plot. The measured kinetic exponent is $z = 0.74 \pm 0.05$ in each case. This value of z is rather similar to the 2D scaling result in the intermediate regime mentioned above [28] and also to the kinetic exponent obtained in large-scale 2D DLCA simulations [31] with a fair degree of cluster crowdedness. This agreement strongly indicates that fragmentation does not play an important role over the simulation time for these choices of the potential well depth.

The kinetic exponent z can be alternatively obtained by measuring the temporal evolution of the mean cluster radius of gyration $\langle R_g \rangle$. In the scaling description of DLCA, $\langle R_g \rangle \sim t^a$ with $a = z/D_f$. Therefore, if fractal dimension D_f is known, z can be deduced from a log-log plot of $\langle R_g \rangle$ vs time t. In Fig. 7 we show such a log-log plot for various values of $|U_m|$. For computing $\langle R_g \rangle$, we only use clusters containing more than four particles. For both $|U_m| = 6.0$ and $7.0 k_B T$ we obtain $a = 0.52 \pm 0.04$, which yields $z = 0.73$ for $D_f = 1.4$. Thus, both methods of measuring the kinetic exponent z show good agreement with each other for deep well depths.

(b) Shallow quench in the two-phase region. For shallower well depths in the two-phase region, fragmentation of clusters can take place. However, it is expected that fragmentation predominantly occurs at the surface of the cluster; this is the celebrated evaporation-condensation mechanism behind Ostwald ripening [32]. In addition, surface reorganization of clusters can take place to reduce interfacial tension. One of the most important characteristics of cluster growth under spinodal decomposition is that the clusters are compact and, as a result, both cluster nearest-neighbor separation R_{nn} and the cluster radius-of-gyration R_g grow with the *same* temporal exponent. In other words, there is only one length scale in the system. The growth law in these cases can be generally written as $R_g(t) \sim t^n$. It is well established [4] that $n = 1/3$ at late times in both two and three dimensions, while at intermediate times, dominated by surface diffusion and coalescence of diffusing clusters, the growth-law exponent can be characterized [32,33] by $n = 1/4$. We have plotted a log-log graph of $\langle R_g \rangle(t)$ vs t in Fig. 8 for two shallower well depths inside the two-phase coexistence. In each case, at intermediate times (when the average radius of gyration of clusters $\simeq 5$ or bigger), we observe the growth of clusters characterized by an exponent of $\approx 1/4$. We have checked that both R_g and R_{nn} do increase proportionately with each other at these times. For $|U_m| = 3.5 k_B T$, we also observe a *nucleation induction time* at the very beginning, after which cluster growth and coarsening take place.

(c) Quench in the single-phase region. In the presence of fragmentation, Sorensen, Zhang, and Taylor (SZT) [34] have generalized the Smoluchowski equation on the assumption that both the aggregation and fragmentation kernels are homogeneous functions [35,36]. SZT arrives at a general expression for the evolution of the mean cluster size in terms of reduced variables $s^* = s/s_o$ and $t^* = t/t_o$,

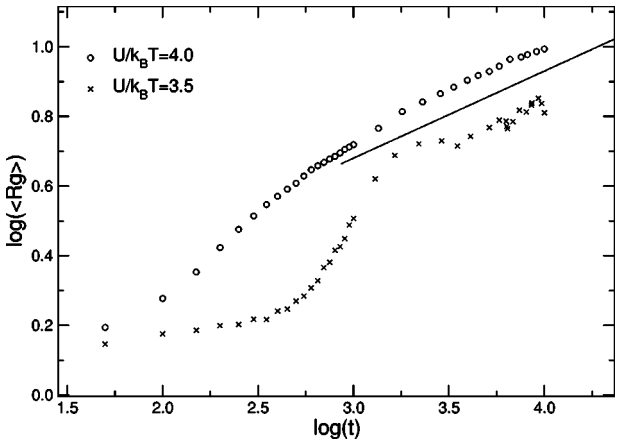

FIG. 8. Log-log plot of radius of gyration vs time for shallower well depths in the two-phase region. The solid line is a guide to the eye with a slope of $1/4$. Cluster growth at intermediate times is consistent with $R_g(t) \sim t^n$, with $n \approx 0.25$.

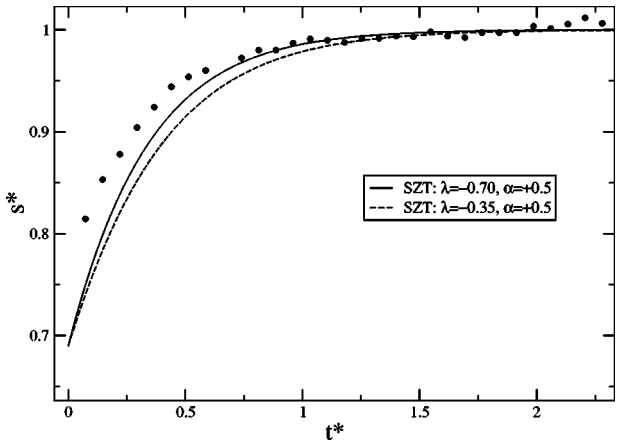

FIG. 9. Comparison between simulation results for growth kinetics in the single phase and SZT prediction for two sets of parameter values. Here, $|U_m|=2.0k_BT$.

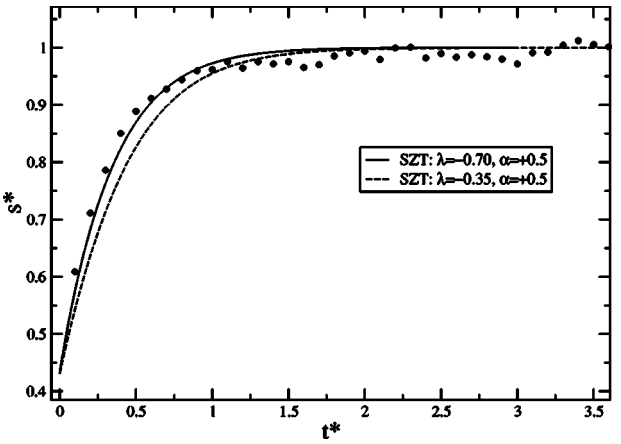

FIG. 10. The same as in Fig. 10, except $|U_m|=3.125k_BT$ here.

$$\frac{ds^*}{dt} = s^{*\lambda} - s^{*\omega+2}, \tag{6}$$

where s_o is the steady-state value of $s(t)$ at long time, and t_o is a characteristic time scale for the approach to equilibrium. The exponents λ and ω stand for the degree of homogeneity of the aggregation and fragmentation kernels, respectively. It is clear from our discussion above that the SZT description of aggregation fragmentation is not applicable in the two-phase region, where the cluster size increases indefinitely in the thermodynamic limit. However, in the single-phase region, where the clusters grow only up to the size of the correlation length, the SZT equation might have a limited validity. We numerically solve this first-order SZT differential equation [Eq. (6)] with the initial condition $s^*(t=0)=1/s_o$. It is not immediately clear what values of λ and ω to substitute in Eq. (6). As we have discussed, in the dilute limit of the DLCA model $z=0.59$, hence $\lambda=-0.7$, while for a moderate value of cluster crowdedness, z increases to 0.74 in the simulations and the corresponding λ becomes −0.35. We choose $\omega=1/2$ in the mean-field model of SZT to roughly incorporate the possibility that cluster fragmentation happens mostly at the surface. As mentioned, we consider two neighboring particles to belong to the same cluster if the distance between their centers is less than or equal to the range of the interaction. A comparison with the SZT prediction in the single phase is carried out in Figs. 9 and 10 for $|U_m|=2$ and $|U_m|=3.125k_BT$, respectively. In these figures we show SZT predictions along with our simulation results for both $\lambda=-0.35$ and −0.7 and $\omega=1/2$. It is clear that $\lambda=-0.7$ shows excellent agreement with the simulation data. This is perhaps due to the fact that the average cluster sizes are relatively small throughout the simulation time and cluster crowding does not substantially modify the dilute limit values of z and λ. Thus, it is appropriate to substitute the dilute limit value of $\lambda=-0.7$ in the SZT model for a comparison with these simulation results.

3. Cluster size distribution

To characterize the cluster size distribution, we invoke a standard scaling ansatz applicable in many physical situations [32,37], where cluster distributions are assumed to obey a scaling law given by

$$n(N,t) = \frac{N_m}{s(t)^2}\phi\left(\frac{N}{s(t)}\right), \tag{7}$$

where N_m stands for the total number of particles (monomers) in the system and $\phi(N/s)$ is a general scaling function. The scaling form assumed for the cluster size distribution [Eq. (7)] is tested in Figs. 11 and 12 for $|U_m|=7$ and $3.5k_BT$, respectively. Results are averaged over more than 100 runs. The prescribed scaling form seems to work well for $|U_m|=7k_BT$. For such a deep well depth, one would expect that fragmentation of clusters will be rare and a comparison with DLCA simulations will be meaningful over the simulation time. For DLCA, the scaling function can be expressed as [37]

$$\phi(x) = Ax^{-\lambda}e^{-\alpha x} \tag{8}$$

for large values of the scaling variable $x=N/s$. Here, $\lambda=1-z^{-1}$ and $\alpha=1-\lambda$. If we consider $z=0.74$ appropriate for this deep well depth (see Fig. 7), we find $\lambda=-0.35$ and $\alpha=1.35$.

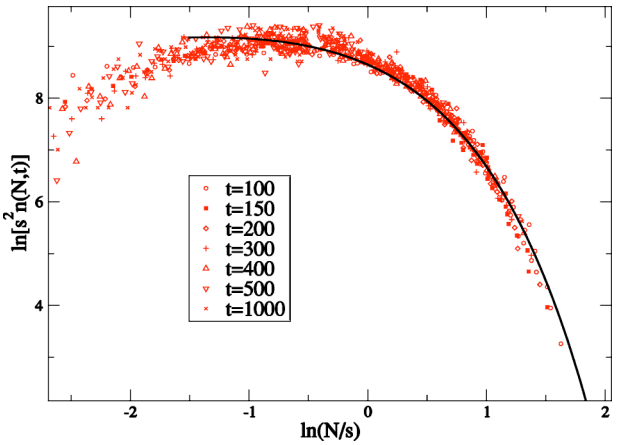

FIG. 11. Scaling of the cluster size distribution for $|U_m|=7.0k_BT$. The results are averaged over 150 runs. The solid line is fit to the data according to Eq. (8) with $\lambda=-0.35$ and $\alpha=1.35$ for scaling variable $N/s\geqslant 1$.

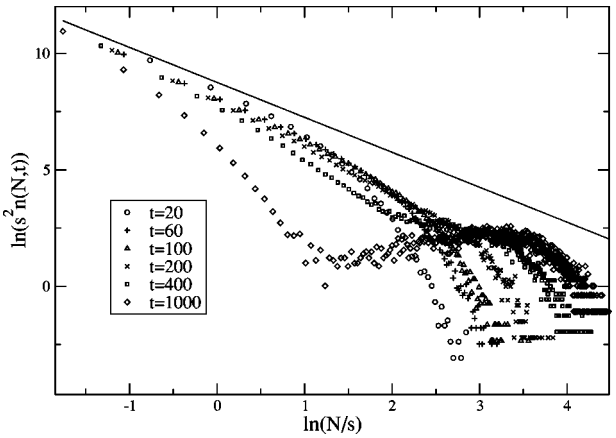

FIG. 12. Scaling of the cluster size distribution for $|U_m|=3.5$. The results are averaged over 100 runs. A solid line of slope −1.5 is added to guide the eye.

Figure 11 shows that Eq. (8) with these values of λ and α fit the scaled cluster size distribution quite well for large values of x.

Scaling does not seem to work so well for $|U_m|=3.5k_BT$ (Fig. 12). For small values of the scaling variable and at earlier times, a power law with an exponent close to −1.5 is found in the scaling function. Such a power-law decay of scaling functions are reminiscent of a RLCA behavior. We should point out that a similar exponent of −1.5 has been observed by Hobbie [12] in the scaling function for a binary colloidal mixture in which depletion forces arise from the difference in size between two colloids. The origin of the RLCA-type power-law behavior for this shallow well depth is perhaps due to the fact that clusters do not stick the first time they approach each other. There is also a hint of an exponential decay in the size distribution for large x as seen by Hobbie. At later times, the "scaling function" changes appreciably, displaying the presence of a broad maximum at an intermediate value of N/s.

IV. CONCLUDING REMARKS

To provide a unifying description of the transition from the dispersed to the solid phase (which includes both fractal and crystalline aggregates), we have carried out a detailed study of the kinetics of phase transformations in a model 2D colloidal system. The interaction among colloidal particles in this work arises from the depletion effect due to the addition of a nonadsorbing polymer, and is modeled as an effective two-body potential. Although the depletion force is assumed to be instantaneous in this work, recent work [38] shows that the depletion force will have a time dependence that will in general affect colloidal kinetics. However, this time dependence is quite weak for the size parameter ζ used in our work. Thus, we do not expect this to substantially change our conclusions.

Large-scale morphology of clusters obtained in the simulation show good agreement with those observed by Hoog *et al.* [13] in their experimental work on depletion-driven colloids. We characterize the morphology of clusters for various values of the magnitude of the potential well depth $|U_m|$. There exists a critical value of this well depth (U_c) in the model. When $|U_m|<U_c\simeq 3.130k_BT$, the system remains in a single phase (for our chosen value of the monomer area fraction f) characterized by a dispersed phase of monomers and small clusters. A transition from this dispersed phase to a two-phase coexistence takes place when the system is quenched, such that $|U_m|>U_c$. In the two-phase region, a dispersed and hexagonally packed crystal phase can coexist. Gradual transition from round cluster growth to the formation of elongated clusters is observed as the well depth is increased. Increasing the well depth even more, fractal clusters are observed in the simulation. These fractal clusters have a hybrid nature in the sense that the aggregates show hexagonal closed-packed crystalline ordering at short length scales and a ramified fractal nature at larger length scales. For sufficiently deep potential wells, the large-scale fractal dimension of the clusters are close to those obtained in simulations of DLCA model in two dimensions, $D_f\simeq 1.4$.

Further quantitative comparisons with the DLCA model are carried out next in the limit of deep potential well depths. Kinetic exponents obtained from both the mean number of particles in a cluster and the average cluster radius of gyration provide strong support that the DLCA limit in the kinetics can be achieved for deep potential wells. In addition, the scaling function for cluster size distribution matches the DLCA scaling form for deep potential well depths. For shallower well depths in the two-phase region, growth kinetics is compared with early-time theories of phase separation. In the single-phase region, comparison of simulation results with a mean-field aggregation-fragmentation model shows good agreement.

Our work clearly demonstrates the importance of Brownian dynamics simulations in the study of colloidal aggregation, and more generally, for studying the transition from a dispersed to a solid phase. Past theoretical studies of fractal aggregates in colloids, for example, typically started from the DLCA model, which turns out to be the irreversible limits of our simulation and are recovered for a deep well depth. In contrast, aggregates that cross over from fractal to compact crystalline morphology can be easily studied in Brownian dynamics simulations by changing a simple parameter of the model. More importantly, growth kinetics and aggregate size distributions that evolve from nonequilibrium to equilibrium limits can be accessed in a reasonable amount of computer time. We expect that our results would stimulate further theoretical and experimental studies towards the understanding of the transition from a dispersed to a solid phase in widely different physical situations.

ACKNOWLEDGMENTS

J.J.C. and T.S. acknowledge financial support from the Spanish MCyT through Grant No. BMF2001-0341-C02-01. A.C. and C.S.were supported by NASA through Grant No. NAG 3-2360. J.J.C. thanks Professors A. Chakrabarti and C. Sorensen for the warm hospitality shown during his visit to Kansas State University.

[1] *Kinetics of Aggregation and Gelation*, edited by F. Family and D. Landau (North-Holland, Amsterdam, 1984).
[2] S. K. Friedlander, *Smoke, Dust and Haze* (Oxford, New York, 2000).
[3] P. Meakin, J. Sol-Gel Sci. Technol. **15**, 97 (1999).
[4] For a review, see, for example, A. J. Bray, Adv. Phys. **43**, 357 (1994).
[5] A. G. Walton, *The Formation and Properties of Precipitates* (Interscience, New York, 1967); A. E. Nielsen, *Kinetics of Precipitation* (Pergamon, Oxford, 1964).
[6] For a review, see W. C. K. Poon and M. D. Haw, Adv. Colloid Interface Sci. **73**, 71 (1997).
[7] For a review, see, V. J. Anderson and H. N. W. Lekkerkerker, Nature (London) **416**, 811 (2002).
[8] J. Israelachvili, *Intermolecular and Surface Forces* (Academic, San Diego, 1994).
[9] S. Asakura and F. Oosawa, J. Chem. Phys. **22**, 1255 (1954).
[10] A. Vrij, Pure Appl. Chem. **48**, 471 (1976).
[11] R. Verma, J. C. Crocker, T. C. Lubensky, and A. G. Yodh, Macromolecules **33**, 177 (2000).
[12] E. K. Hobbie, Phys. Rev. Lett. **81**, 3996 (1998).
[13] E. H. A. de Hoog, W. K. Kegel, A. van Blaaderen, and H. N. W. Lekkerkerker, Phys. Rev. E **64**, 021407 (2001).
[14] P. N. Segrè, V. Prasad, A. B. Schofield, and D. A. Weitz, Phys. Rev. Lett. **86**, 6042 (2001).
[15] A. M. Puertas, M. Fuchs, and M. E. Cates, Phys. Rev. Lett. **88**, 098301 (2002).
[16] A. J. Liu and S. R. Nagel, Nature (London) **396**, 21 (1998).
[17] K. G. Soga, J. R. Melrose, and R. C. Ball, J. Chem. Phys. **108**, 6026 (1998).
[18] K. G. Soga, J. R. Melrose, and R. C. Ball, J. Chem. Phys. **110**, 2280 (1999).
[19] R. J. M. d'Arjuzon, W. Frith, and J. R. Melrose, Phys. Rev. E **67**, 061404 (2003).
[20] D. Costa, P. Ballone, and C. Caccamo, J. Chem. Phys. **116**, 3327 (2002).
[21] W. F. van Gunsteren and H. J. C. Berendsen, Mol. Phys. **45**, 637 (1982).
[22] N. Q. Nguyen and A. J. C. Ladd, Phys. Rev. E **66**, 046708 (2002);J. F. Brady, J. Chem. Phys. **99**, 567 (1993);D. O. Reese *et al.*, Phys. Rev. Lett. **85**, 5460 (2000).
[23] J. R. Melrose, Europhys. Lett. **19**, 51 (1992).
[24] M. Dijkstra, J. M. Brader, and R. Evans, J. Phys.: Condens. Matter **11**, 10079 (1999).
[25] V. J. Anderson, E. H. A. de Hoog, and H. N. W. Lekkerkerker, Phys. Rev. E **65**, 011403 (2001).
[26] A. T. Skjeltorp, Phys. Rev. Lett. **58**, 1444 (1987).
[27] J. M. Victor and J. P. Hansen, J. Phys. (France) Lett. **45**, L-307 (1984).
[28] A. Chakrabarti, D. Fry, and C. M. Sorensen, Phys. Rev. E (in press).
[29] M. Kolb, Phys. Rev. Lett. **53**, 1653 (1984).
[30] D. Fry, T. Sintes, A. Chakrabarti, and C. M. Sorensen, Phys. Rev. Lett. **89**, 148301 (2002).
[31] D. Fry, Ph.D. thesis, Kansas State University, 2003.
[32] J. Gunton, M. San Miguel, and P. S. Sahni, in *Phase Transitions and Critical Phenomena*, edited by C. Domb and J. L. Lebowitz (Academic, London, 1983), Vol. 8.
[33] D. A. Huse, Phys. Rev. B **34**, 7845 (1986).
[34] C. M. Sorensen, H. X. Zhang, and T. W. Taylor, Phys. Rev. Lett. **59**(3), 363 (1987).
[35] F. Family, P. Meakin, and J. M. Deutch, Phys. Rev. Lett. **57**, 727 (1986).
[36] T. Sintes, R. Toral, and A. Chakrabarti, Phys. Rev. A **46**, 2039 (1992).
[37] P. G. J. van Dongen and M. H. Ernst, Phys. Rev. Lett. **54**, 1396 (1985).
[38] G. A. Vliegenthart and P. van der Schoot, Europhys. Lett. **62**, 600 (2003).